Study of the Bucket Design Effect on Static Torque of Unconventional Savonius Wind Rotors for Low-Velocity Ranges

Youssef Kassem [1,2]* and Hüseyin Çamur[1], and Almonsef Mosbah[1]

[1]*Department of Mechanical Engineering, Faculty of Engineering, Near East University, 99138 Nicosia, Cyprus.*
[2]*Department of Civil Engineering, Faculty of civil and Environmental Engineering, Near East University, 99138 Nicosia, Cyprus.*

Abstract

The main objective of this paper is to increase the low performance of the unconventional Savonius vertical-axis wind rotor turbine. Three configurations (model 1, 2 and 3) of Savonius rotor were designed for the selected arc bucket angles of 60°, 75° and 90°. The effect of bucket angles on the rotor performance was analyzed both experimentally and numerically. The rotor performance was obtained through the static torque for each model. The static torque at different rotor angles ranging from 0º to 180º was studied at various wind speeds of 4, 6 and 8 m/s. The experimental investigations on unconventional Savonius rotors were conducted in an open wind tunnel. Numerical models used are the software SolidWorks Flow Simulation (SWFS) and Trigonometric Fourier Series (TFS). By comparing the numerical and experimental results it can be concluded that the rotor of arc bucket angle of 90° gives the best performance at higher wind speed than the other two models for all rotor angles. Moreover, the comparison between the numerical analysis and the global experimental results confirms the validity of the numerical methods. The overall reliability of the results for unconventional Savonius wind turbines was achieved. The research contributes to design, construct, and manufacture the Savonius wind turbines at low-cost to generate electricity for household in Cyprus.

Keywords: Arc angle; Cyprus; Savonius rotor; SWFS; TFS; Torque

NOMENCLATURE :

C	Chord, mm
C_B	Constant of the k-ε turbulence model, dimensionless
$C_{1\varepsilon}$	Constant of the k-ε turbulence model, dimensionless
$C_{2\varepsilon}$	Constant of the k-ε turbulence model, dimensionless
C_μ	Constant of the k-ε turbulence model, dimensionless
F	Force acting on the rotor shaft, N
F_i	Force per volume, N.m⁻³
f_1	Lam and Bremhorst damping function
f_2	Lam and Bremhorst damping function
f_μ	Lam and Bremhorst damping function
G_k	Production term of turbulence
g	Gravitational acceleration, m/s²
H	Blade height, mm
k	Turbulent kinetic energy, J.kg⁻¹
l	Length, m
m	Mass loaded on the pan, kg
N	Number of blades
P	Pressure, Pa
P_B	Constant of the k-ε turbulence model, dimensionless
r_{shaft}	Radius of the shaft, m
r_{rope}	Radius of the nylon string, m
S	Spring balance reading, kg
s_{ij}	Component of the strain rate tensor, s⁻¹
T	Static torque, N.m
T	Periodic fucntion, s
u_i	Velocity components, m.s⁻¹
u_i'	Fluctuating velocity components, m.s⁻¹
u_j	Velocity components, m.s⁻¹
u_j'	Fluctuating velocity components, m.s⁻¹
u_k	Fluctuating velocity components, m.s⁻¹
V	Magnitude velocity, m.s⁻¹
X	Cartesian coordinate, m
x_i	Cartesian coordinate, m
x_j	Cartesian coordinate, m
x_k	Cartesian coordinate, m
Y	Cartesian coordinate, m
Y	Distance from point to the wall, m
Z	Cartesian coordinate, m
ε	Dissipation rate of the turbulent kinetic energy, W.kg⁻¹
M	Dynamic viscosity, Pa.s
μ_t	Turbulent viscosity, Pa.s
ρ	Density, kg.m⁻³
σ_ε	Constant of the k-ε turbulence model
σ_k	Constant of the k-ε turbulence model
σ_B	Constant of the k-ε turbulence model
φ	Bucket arc angle, °
δ_{ij}	Kronecker delta function, dimensionless
τ_{ij}	Laminar stress tensor
τ_{ij}^R	Reynolds stress tensor

1. INTRODUCTION

Numerous studies of the vertical axis wind turbine were carried out based upon the Savonius wind turbine which was invented in 1992. A Savonius rotor is a drag-type turbine and the conventional Savonius wind rotor is consisted of two semi-cylindrical blades perpendicular to the wind direction [1, 2] with the advantages of simple design and low construction cost. It is generally used for various purposed [3]. Otherwise, the design and analysis of this rotor have aroused a large credit, not only in research and academic communities but also in industrial appliances. Comparing to other types of vertical axis wind turbine, Savonius wind turbine has lower efficiency. Because of the one blade is moved against the wind when another one moves in the direction of the wind [4, 5]. Savonius rotor is closely related to torque and most investigations have been focused on experimental and numerical studies related to the aerodynamic characteristics and the effects of blade geometries.

Intensive studies on the optimization of Savonius wind turbine rotors have been conducted based on an experimental work and numerical analysis [6-20]. For example, Akwa et al. [17] examined numerically the effect of the overlap ratio of a Savonius rotor on the averaged moments and power coefficients, over complete cycles of operation. The authors concluded that the buckets overlap over the rotor indicates that the maximum device performance occurs for buckets overlap ratios with values close to 0.15. Driss et al. [18] investigated experimentally the external overlap ratios effect on the performance of a vertical axis wind rotor of the Savonius type. He concluded that with the increase of the external overlap value, the torque and power coefficients decrease. Mohamed et al. [19] studied various shapes of obstacles and deflectors placed in front of Savonius turbine with two and three blades. A rounded deflector structure was placed in front of two counter-rotating turbines. Wenehenubun et al. [20] studied experimentally the effect of number of blades on the performance of the model of the Savonius type wind turbine. He investigated numerically the pressure distribution of the turbine. They both reported that Savonius model with three blades has the best performance at high tip speed ratio.

Furthermore, numerical techniques have been overwhelmingly used in the study of the curved blade Savonius wind rotors [21-25]. Regarding the numerical study using SolidWork Flow Simulations with the steady Reynolds average Navier-Stokes (k-ε RNG) model, some recent papers, simulated unconventional Savonius wind rotors. For example, Driss et al. [26] studied the bucket design effect on the turbulent flow around new configuration of Savonius wind rotors. The study compared different rotors having different arc bucket angels equal to 60°, 75°, 90° and 130° when keeping constant geometrical parameters. In their study, they observed that the depression zones increase with the increase of the bucket arc angle. Driss et al. [27] investigated numerically and experimentally the turbulent flow around a small incurved Savonius wind rotor. They both agreed that incurved Savonius wind rotor has an effect on the local characteristics. Frikha et al. [28] studied numerically and experimentally the effect of five configurations with the

different number of stages on the performance of a Savonius rotor. Based on their results, the number of stages affects the aerodynamic behavior of the turbulent flow around the Savonius rotor. And, it showed that the dynamic torque coefficient and the power coefficient increase when the number of stage increases.

On the basis of the previous studies, the importance of studying the static torque of a new design to improve the performance of the conventional Savonius wind rotor are revealed since it directly affects the efficiency of rotors. Although Savonius wind rotor promises to generate positive static torque coefficients, there is no information on the characteristics of static torque measurements related to new design of conventional Savonius rotors in the open literature. Savonius wind turbines have low cut-in speeds and can be operated at low wind speeds. The wind speeds recorded according to meteorological statistics in Cyprus are in the range of 4-8 m/s. Therefore, in the present study, new configurations of Savonius wind turbine were selected for the investigations on performance improvements. Hence, authors of this study developed experimental and numerical investigations to study the static torque characteristics. In the present paper, three different models (model 1, 2 and 3) of unconventional Savonius wind turbine rotors with different arc bucket angles are introduced. The aim of the work is to study the bucket arc angle effect on the static torque characteristics of each new rotor configuration at low wind speeds (4-8 m/s). For the experimental study, test rig shown in Figure 2 was established and for numerical study, the SWFS software program and TFS are utilized. The buckets used in the experiments are both simple and cheap as they are made of light plastic (PVC) tubes. This work was mainly conducted to optimize the new configuration of unconventional Savonius rotor with the intention of proving information for simple vertical axis machines which could be manufactured at low cost. The performance of this simple machine can be improved by investigating the new configurations and they can be manufactured for the consumers in Cyprus.

The paper is organized in the following manner: Section 2 outlines the basic description of the experimental method with various arc bucket models. Section 3 describes in detail the most important concepts of the numerical models for static torque analysis. Section 4 explains the effect of various arc bucket angles and wind speeds on the static torque of Savonius rotors, and Section 5 gives the major conclusions.

2. MATERIAL AND METHOD

This section focuses on the experimental study of the arc bucket angle effect on the static torque characteristics of unconventional Savonius rotors (model 1, 2 and 3) for different rotor angles at various wind speeds. Following sections will summarize the arc bucket models used, the experimental setup and method.

2.1 Unconventional Savonius Wind Rotor

In experiments, unconventional Savonius rotor is used for converting the force of the wind into torque on a rotating

shaft. The shaft and blades of the unconventional Savonius rotor are made of galvanized steel and PVC material, respectively. For this reason, the materials were selected to avoid structural failure of the wind turbine due to the forces that winds would impose on the blades. The thickness of the blades is 6 mm, which makes the Savonius rotor design economical and efficient [26]. Figure 1 presents the configuration of three different bucket geometries that are used in the current study. In addition, the dimensions of unconventional Savonius vertical axis wind rotor for three different models are shown in Table 1.
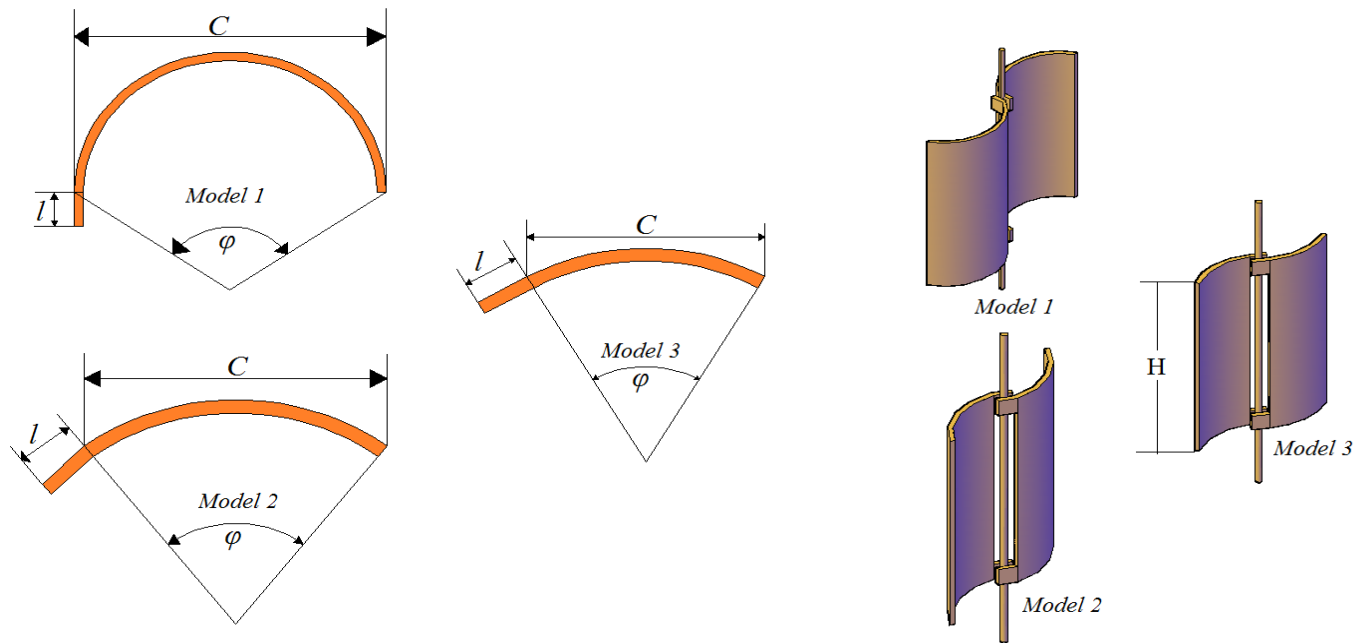
Figure 1. Geometries of Savonius rotors

Table 1. Different fixed and variable parameters considered in the design analysis

Category	Design parameter		Value	
Physical features	1.	Blade	With different shape	
			Model 1	90°
		φ	Model 2	75°
			Model 3	60°
	2.	Number of blades (N)	$N = 2$ blades	
Dimensional	3.	Chord (C)	$C = 100$ mm	
	4.	Blade height (H)	$H = 300$ mm	
	5.	Plate length (l)	$l = 24$ mm	
Operational	6.	Rated wind speed (V)	$V = 4, 6$ and 8 m/s	

2.2. Wind Tunnel

The overall design of the open wind tunnel is presented in Figure 2. Uniform main flow is introduced by an open wind tunnel with a wind speeds up to 15 m/s at the tunnel exit. Air exits from a square contraction nozzle with a wind tunnel outlet of 400 mm × 400 mm. The support eliminates all kinds of vibration and ensures a good stability of the tunnel during the experimental tests.

2.3. Experimental Setup

The experimental setup utilized in present study was developed according to previous study [10, 29]. Figure 2 shows the schematic diagram of experimental set-up used in this study. Experimental set-up consists of a structure which houses the Savonius rotor made-up by using studs and wood frames. The tested rotors are supported vertically in wood housing as shown in Figure 2. The Savonius rotor is connected to the shaft of the rotor by bolts facilitating easy

replacement of rotors. Two bearings bolted into the wood plates support the Savonius rotor. The blade of the rotor is connected to the shaft by bolts. The usage of studs, nuts and bolts facilitated easy replacement of rotors of different blade shapes and positioning of the rotor center at the center of the wind tunnel. The weighing pan, pulley and electronic spring are connected and balanced by a fishing nylon string of 1 mm diameter. The important parameter may affect the measurements of static torque of the rotor is friction of

bearings and wire. Therefore, in this study nylon wire of 1 mm were used. In addition, the two bearing are washed with petrol to remove the grease and seals are removed also to minimize the friction of bearings.

The turbine captures wind and moves due to the presence of drag forces, which cause to rotate the shaft around its fixed axis as shown in Figure 2. The support eliminates all kinds of vibration and ensures a good stability of the setup during the experimental tests.
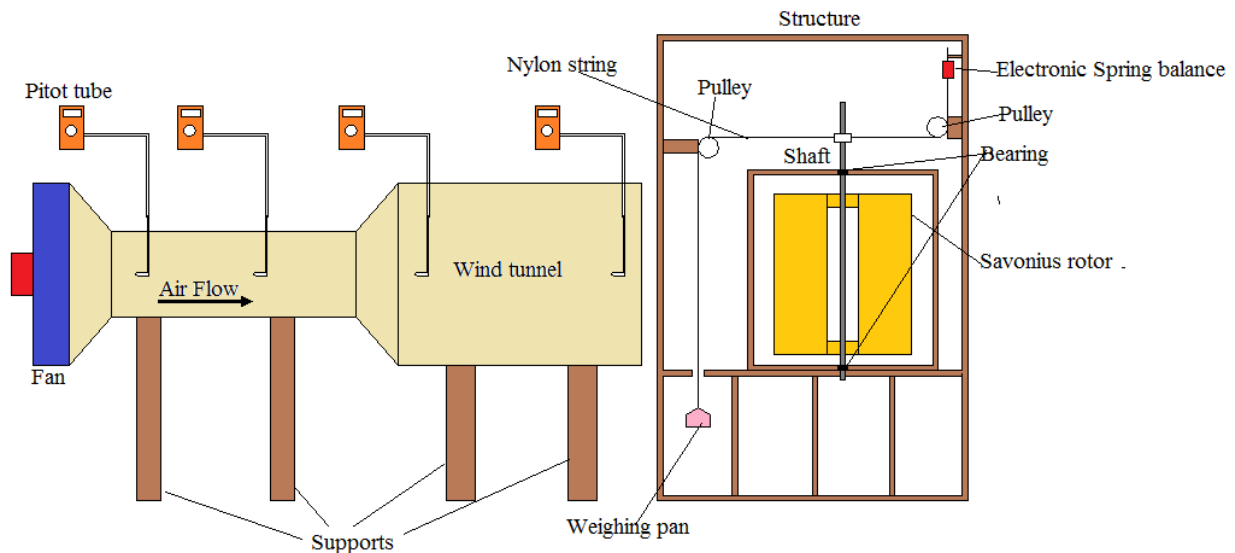

Figure 2. Schematic diagram of the set-up

2.4. Experimental Method

The rotors to be tested are placed at a distance of 750 mm downstream of the wind tunnel nozzle exit such that the center of the stationary or rotating rotor is in line with the center of the wind tunnel exit. Four Pitot tube were used to measure the wind speed in different positions with an accuracy of 0.1 m/s to ensure the velocity of the fan is uniform (Figure 2). The measured velocity distribution at the rotor position is uniform within 3% in the central area of 300 mm× 300 mm. The static torque of the rotors at different rotor positions is determined using a brake drum measuring system. The static torque of the rotor is estimated at rotor positions of ranges 0 to 180 in steps of 30°. The values of load and spring balances reading were recorded at given rotor angle and wind speed to calculate the static torque of the model.

The static torque (T) in unit of Nm of the rotor can be calculates according to [10, 29] using Eq. (1)

$$T = [(m - s)g](r_{shaft} + r_{rope}) \qquad (1)$$

where, m is the load in kg, s is spring balance load in kg, r_{shaft} is the radius of the shaft in m, r_{rope} is the radius of the nylon string in m and g is the gravitational acceleration in m/s^2.

The force (F) acting on the rotor shaft obtained in (N) by:

$$F = (m - s)g \qquad (2)$$

3. NUMERICAL MODELS

In the current study, the static torque of unconventional Savonius rotors of model 1, 2 and 3 at various wind speeds was analyzed using the SWFS and predicted by TFS.

3.1. SolidWorks Flow Simulation (SWFS)

3.1. 1 Mathematical Formulation

The mathematical equations can be defined as a composition of dependent, independent variables and relative parameters in the form of differential equations which govern the physical phenomena. In this study, standard k-ε turbulence model has been used with logarithmic surface function in the analysis of turbulent flow. The Navier-Stokes equations governing the flow of air are obtained from the continuity equation, the equations of momentum, the transport equation of turbulent kinetic energy (k) and the transport equation of dissipation rate of turbulent kinetic energy (ε). SWFS is based on solving Navier-Stokes equations with a finite volume discretization method. The governing equations can be written for incompressible unsteady flow as follows in the cartesian tensor notation [26, 27 30-32]:

The continuity equation is written as follows:

$$\frac{\partial \rho}{\partial t} + \frac{\partial(\rho u_i)}{\partial x_i} = 0 \qquad (3)$$

The momentum equation is written as follows:

$$\frac{\partial(\rho u_i)}{\partial t} + \frac{\partial(\rho u_i u_j)}{\partial x_j} = -\frac{\partial P}{\partial x_i} + \frac{\partial}{\partial x_j}\left[\mu\left(\frac{\partial u_j}{\partial x_j} + \frac{\partial u_j}{\partial x_i} - \frac{2}{3}\delta_{ij}\frac{\partial u_i}{\partial x_i}\right)\right]$$
$$+ \frac{\partial(-\rho\overline{u_i'u_j'})}{\partial x_j} + F_i \tag{4}$$

They appear a number of additional unknown called the Reynolds stresses $\left(-\rho\overline{u_i'u_j'}\right)$ and defined by

$$-\rho\overline{u_i'u_j'} = \mu_t\left(\frac{\partial u_j}{\partial x_j} + \frac{\partial u_j}{\partial x_i}\right) - \frac{2}{3}\rho k\delta_{ij} \tag{5}$$

The Kronecker delta is defined by $\delta_{ij} = 0$ if i≠j elsewhere, $\delta_{ij} = 1$. In the present work, we have used the modified k-ε turbulence model with damping functions proposed by Lam and Bremhorst [33]. The transport equation of the turbulent kinetic energy k is written as follows:

$$\frac{\partial(\rho k)}{\partial t} + \frac{\partial(\rho k u_i)}{\partial x_i} = \frac{\partial}{\partial x_i}\left(\left(\mu + \frac{\mu_t}{\sigma_k}\right)\frac{\partial k}{\partial x_i}\right) + \tau_{ij}^R\frac{\partial u_i}{\partial x_j} - \rho\varepsilon + \mu_t P_B \tag{6}$$

The transport equation of the dissipation rate of the turbulent kinetic energy ε is written as follows:

$$\frac{\partial(\rho\varepsilon)}{\partial t} + \frac{\partial(\rho\varepsilon u_i)}{\partial x_i} = \frac{\partial}{\partial x_i}\left(\left(\mu + \frac{\mu_t}{\sigma_\varepsilon}\right)\frac{\partial\varepsilon}{\partial x_i}\right)$$
$$+ C_{1\varepsilon}\frac{\varepsilon}{k}\left(f_1\tau_{ij}^R\frac{\partial u_i}{\partial x_j} + C_B\mu_t P_B\right)$$
$$- f_2 C_{2\varepsilon}\frac{\rho\varepsilon^2}{k} \tag{7}$$

The laminar stress tensor is defined by:

$$\tau_{ij} = \mu s_{ij} \tag{8}$$

And the Reynolds stress tensor is defined by:

$$\tau_{ij}^R = \mu s_{ij} - \frac{2}{3}\rho k\delta_{ij} \tag{9}$$

where

$$s_{ij} = \frac{\partial u_i}{\partial x_j} + \frac{\partial u_j}{\partial x_i} - \frac{2}{3}\delta_{ij}\frac{\partial u_k}{\partial x_k} \tag{10}$$

$$P_B = -\frac{g_i}{\sigma_B}\frac{1}{\rho}\frac{\partial\rho}{\partial x_i} \tag{11}$$

The turbulent viscosity is defined as follows:

$$\mu_t = \rho f_\mu C_\mu \frac{k^2}{\varepsilon} \tag{12}$$

In the standard k-ε turbulence model, the constants are used $C_\mu, C_{1\varepsilon}, C_{2\varepsilon}, \sigma_k, \sigma_\varepsilon, \sigma_B$ and C_B, and the numerical values of these constant are given in Table 2.

Table 2. Turbulence constants

C_μ	$C_{1\varepsilon}$	$C_{2\varepsilon}$	σ_k	σ_ε	σ_B	C_B	
0.09	1.44	1.92	1.0	1.3	0.9	1 if $P_B > 1$	0 if $P_B < 1$

Lam and Bremhorst damping function f_μ is defined by:

$$f_\mu = (1 - e^{-0.025R_y})^2\left(1 + \frac{20.5}{R_t}\right) \tag{13}$$

where

$$R_y = \frac{\rho\sqrt{k}y}{\mu} \tag{14}$$

$$R_t = \frac{\rho k^2}{\mu\varepsilon} \tag{15}$$

y is the distance from point to the wall and Lam and Bremhorst's damping functions f_1 and f_2 are:

$$f_1 = 1 + \left(\frac{0.05}{f_\mu}\right)^3 \text{ and } f_2 = 1 - e^{R_t^2} \tag{16}$$

Lam and Bremhorst's damping functions f_μ, f_1, f_2 decrease the turbulent viscosity and the turbulent kinetic energy and increase dissipation rate of the turbulent kinetic energy when the Reynolds number R_y based on the mean velocity of fluctuations and the distance from the wall becomes too small. When $f_\mu=1$, $f_1=1$, $f_2=1$, the approach obtains the original k-ε model. This model has been used by Frikha et al. [34] and satisfactory results were obtained.

3.1.2 Boundary Conditions

In this study, 3D simulation was carried out with SWFS. In general, the physical domain is included the geometrical representation and boundary conditions which refers to the simplified form of computational domain. In the present application, the velocity inlet and outlet flow conditions were taken on the left and right boundaries, respectively. The top and bottom boundaries and the sidewalls are in a symmetrical condition. The inlet velocity values are set for 4, 6 and 8 m/s. The outlet pressure is 101.325 kPa, which means that at this zone the fluid exits the model to an area of an atmospheric pressure. The walls of computational domain are considered as wall boundary conditions. The wind speed enters into the box with the size of 350mm x 550 mm x 600 mm, flows through the rotor blade, and then exits out through an outlet. This does set the environmental conditions. The rotor blade is placed in the middle of the box as shown in Figure 3. Internal analysis shows, the computational domain is automatically enveloped the model wall. The velocity inlet and outlet flow

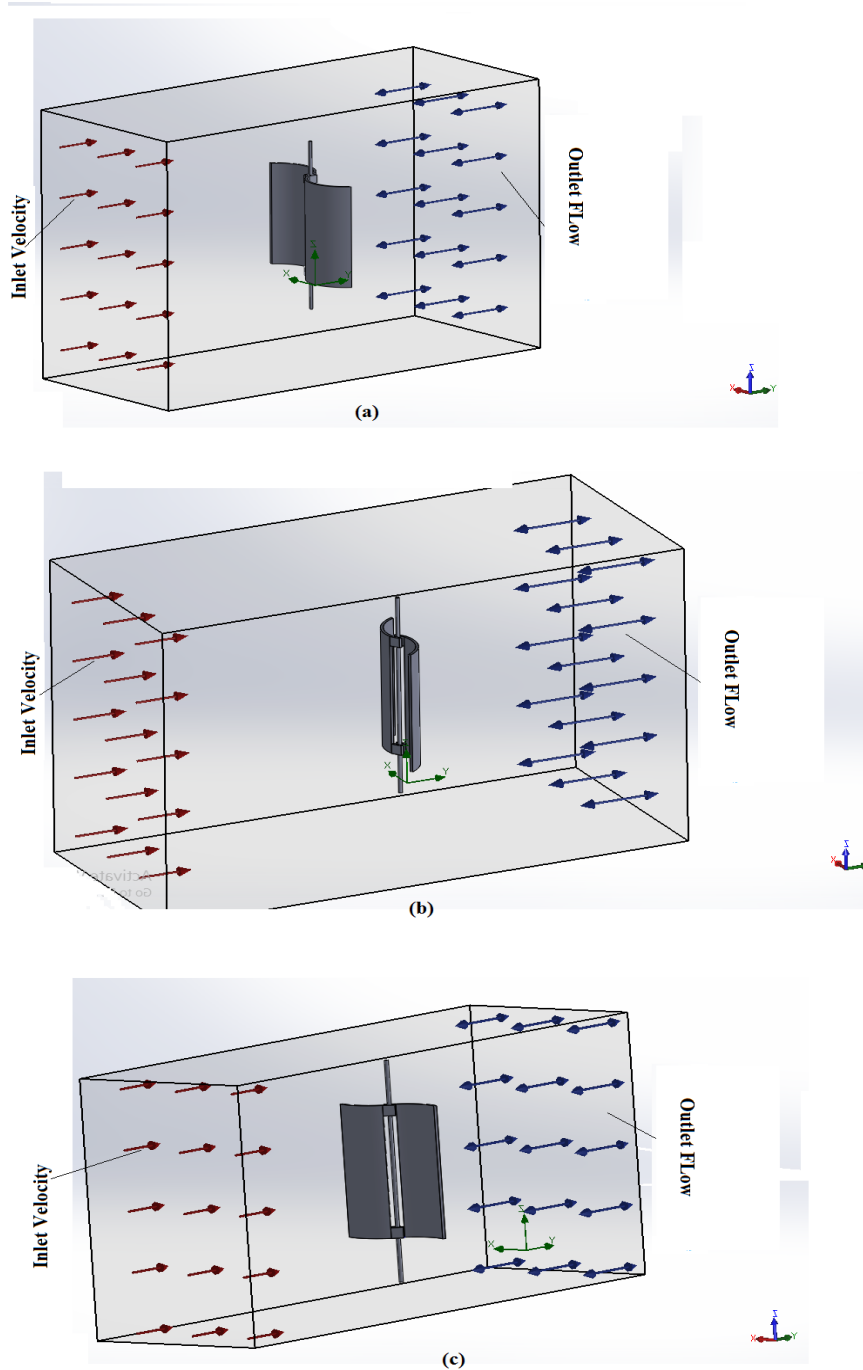were taken for each model left and right boundaries as shown in Figure 3.

Figure 3. Computational domains with boundary conditions for (a) model 1, (b) model 2 and (c) model 3.

3.1.3. Meshing

The process of simulation is repeated with different refinement levels of the mesh. The refinement is carried on undertaking various mesh size and is extended up to a limit after which there is no significant quantitative change in the result. The computational mesh of model 1, 2 and 3 is shown in Figures 4, 5 and 6, respectively. The computational mesh is composed of squared cells and was generated by placing the rotor in a box of 600 mm x 600 mm x 600 mm through which the air flow occurs as shown in Figure 3.
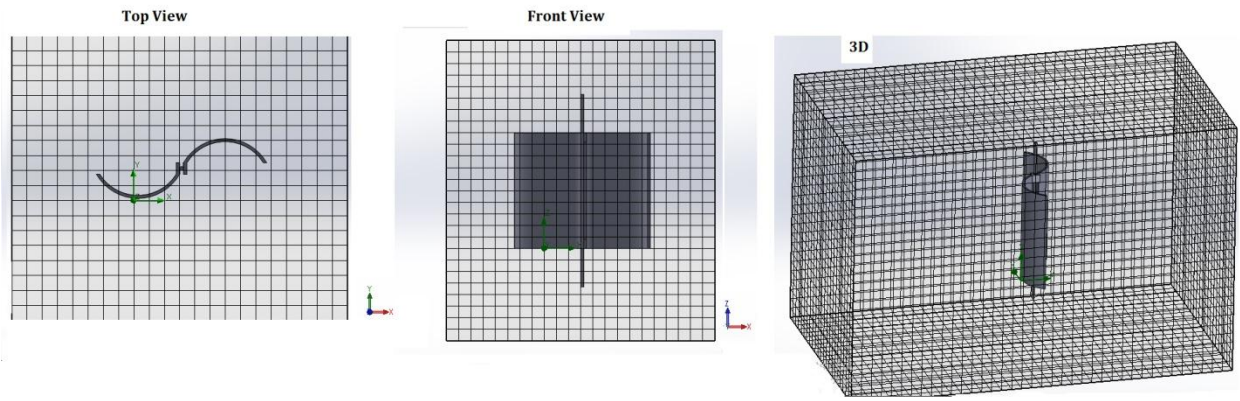
Figure 4. Mesh for Model 1
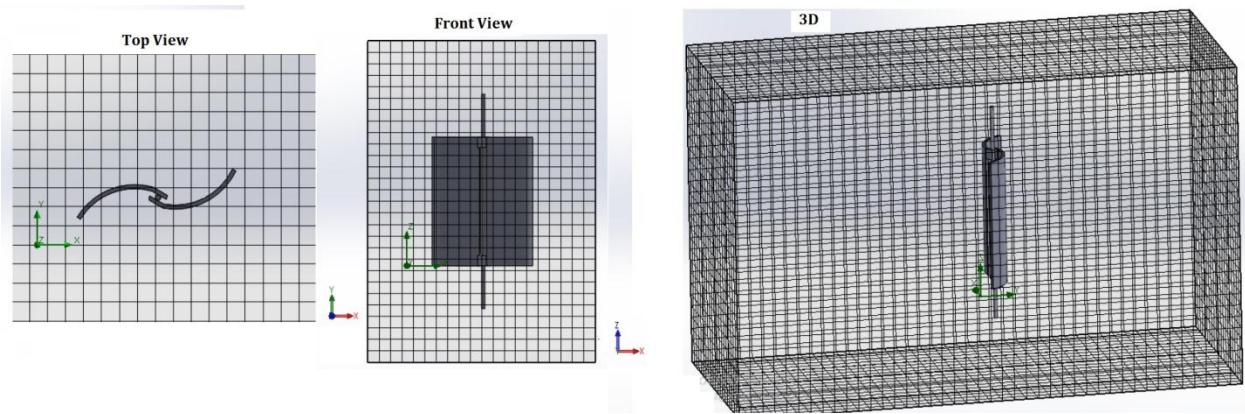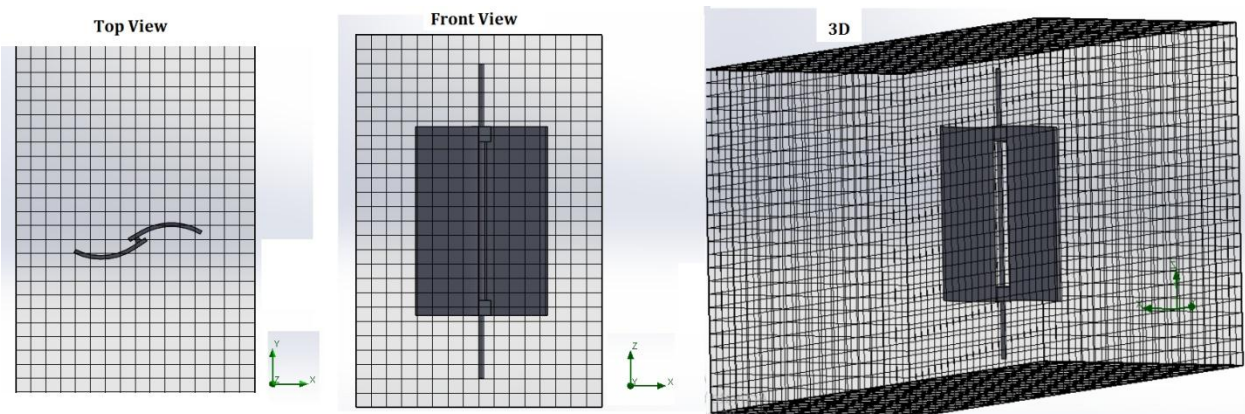

Figure 5. Mesh for Model 2

Figure 6. Mesh for Model 3

The grid independence test was made for improvement of the results by successively using smaller cell sizes grid. The correctness of the results depends largely on the grid's resolution. The grid density is refined up to a certain limit, but beyond this limit, called the grid independent limit, the refinement ceases to significantly affect the results obtained. In fact, the different numbers of mesh cells are used, and the obtained results were compared with the experimental results, to find the optimal number of mesh cells required. It has been observed that when the resolution time increases, the number of mesh cells increases. Indeed, when the cell size increases, the gap between numerical and experimental results increases. Figure 7 shows the various levels of refining using different mesh sizes for the models 1, 2 and 3. Each level was solved in SWFS with the same set of input parameters. After a particular refining limit, the results cease to change. At this point, the grid independence in meshing is said to be achieved. Here, the successful achieved cells are 27684.
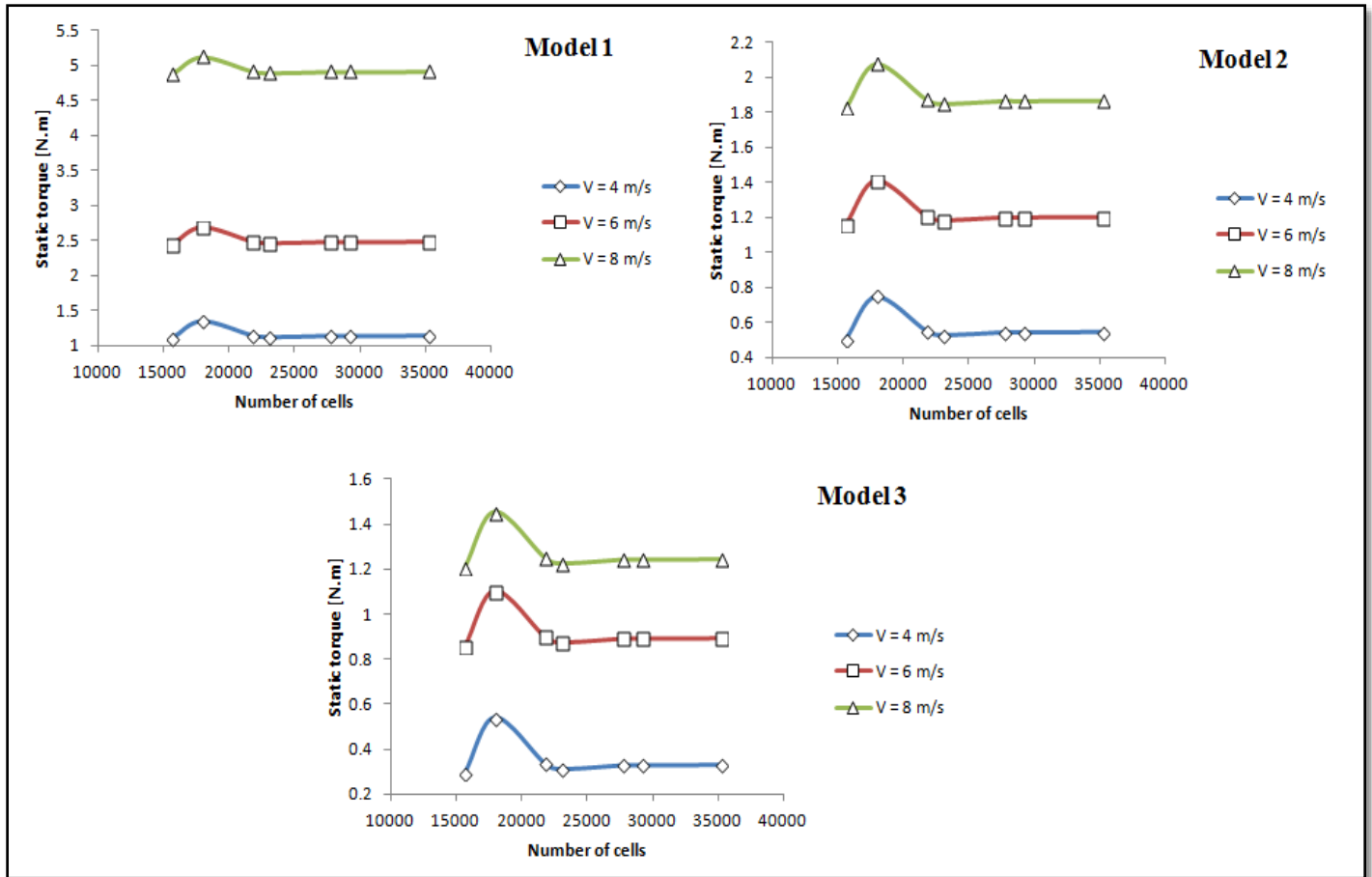
Figure 7. Variation of static torque with respect to number of cells from the grid independence test at rotor angel of 0°

3.2. Trigonometric Fourier Series (TFS)

Fourier series are series of sine and cosine terms. They arise in the representation of periodic functions. A set of harmonically related sine and cosine functions, i.e. $\sin n\omega x$ and $\cos n\omega x$, n = 0, 1, 2 ,…. forms a complete orthogonal set over the interval (0, T) where T =2π/ω. There is a function of y(x) can be represented by a Fourier series comprising the following sine and cosine functions [35]:

$$y(x) = a_0 + \sum_{n=1}^{\infty}\{a_n cos(n\omega x) + b_n sin(n\omega x)\} \qquad (17)$$

This series is called Fourier series and its coefficients are called Fourier coefficients. The fourier coefficients are given by

$$a_0 = \frac{1}{T}\int_o^T y(x)\,dx \qquad (18)$$

$$a_n = \frac{2}{T}\int_o^T y(x)cos(n\omega x)\,dx \qquad (19)$$

$$b_n = \frac{2}{T}\int_o^T y(x)sin(n\omega x)\,dx \qquad (20)$$

where a_0 models a constant term in the data and is associated with $i = 0$ cosine term, ω is the fundamental frequency of

signal, n is the number of terms (harmonic) in the series, and T is periodic function.

4. RESULTS AND DISCUSSIONS

The static torques of the rotors was determined through the experimental and numerical models using experimental measurements, SWFS and TFS. The static torque is obtained by the rotor position ranging from 0° to 180° in steps of 30°. The main features of this work are outlined as follows. Firstly, prototype blades of the models are designed and tested. The experiment carried out in front of an open wind tunnel varying at different wind speed levels. The force acting on the rotor and wind speed were measured and used to determine the static torque of the models.

Secondly, the static torque of models was investigated numerically using SWFS. 3-Dimensional rotor models of various arc bucket angles have been designed in SolidWorks software. Moving mesh and fluid flow simulation have been developed in SWFS. Integration of SWFS and the experimental measurements have made the current research more acceptable and viable. In addition, in order to predict the static torque of the rotors using TFS, rotor angles were used as an input for TFS. As an output static torque is obtained for each model and wind speed. Both studies experimentally and numerically compared through figures.

4.1 Experimental Results

In this investigation, the static torques of the unconventional Savonius rotor using different low wind velocity conditions and arc bucket angles were measured. In accordance with these measurements, the static torque could be deduced in function of the rotor angles.

The results of the experiments indicated the relationship between torque and rotor angle or wind speed are shown in Figures 8, 9 and 10. It is observed that the torque magnitude of three models near the advancing rotor blade tip attains its maximum at a 0° rotor blade angle.

This torque, then decreases until a 45° rotor angle and then starts to increase slightly to reach the peak point at 150°, and then goes down to decrease sharply from (150° to 180°). From these figures, it is observed that the torque of all models increases with the increase in wind velocity. It can also be noticed from the figures that the increase in the bucket arc angle provides a greater available surface area for the wind to push so it would produce more torque. It is evident that a larger bucket arc angle is preferable in the lower range of wind speed for producing maximum torque and better starting characteristics. Thus, with the increase of bucket arc angle (from φ =60° to 90°), the energy capture increases drastically. Therefore, Model 1 has the highest torque compared to other models.
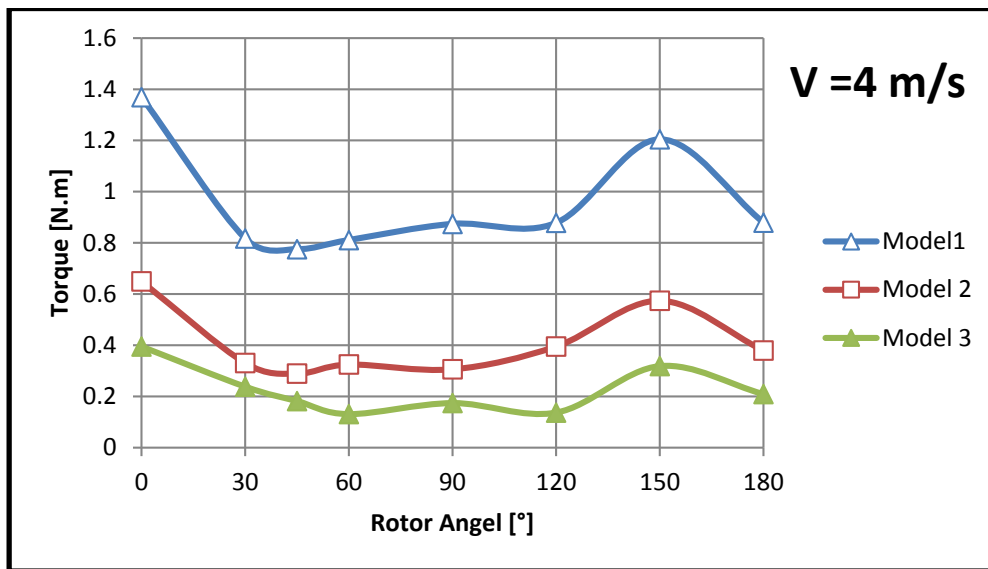

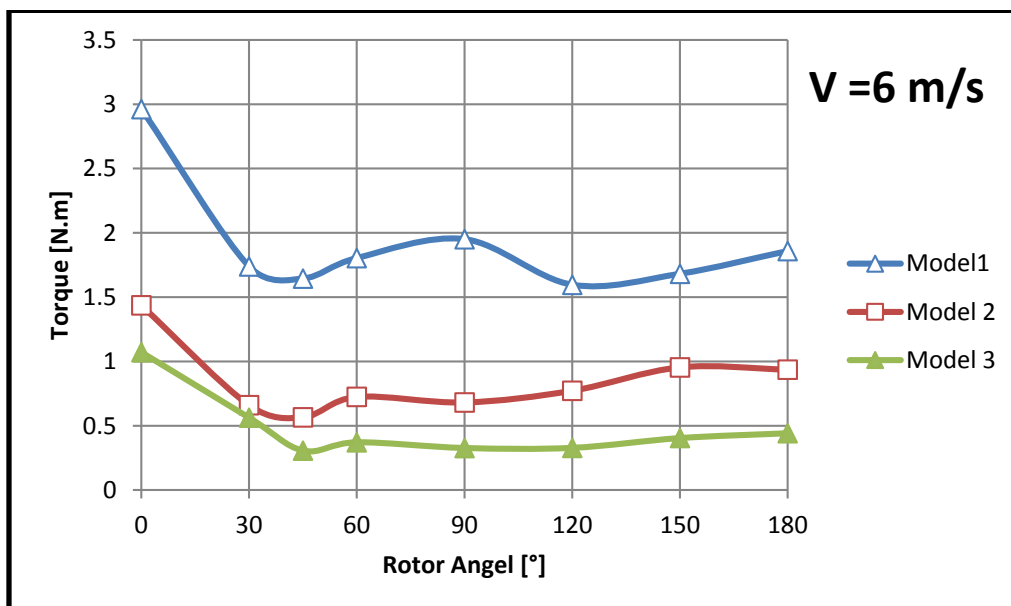**Figure 8.** Static torque variation with angle of rotation at wind speed of 4m/s

Figure 9. Static torque variation with angle of rotation at wind speed of 6m/s
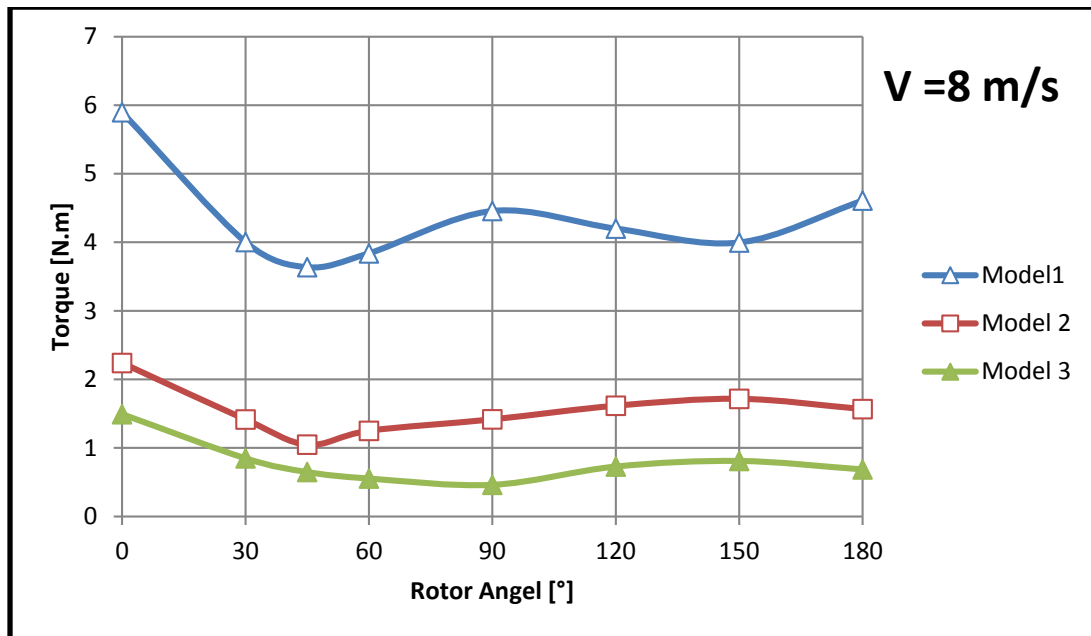
Figure 10. Static torque variation with angle of rotation at wind speed of 8m/s

4.2. Numerical Results

The static torque of unconventional Savonius wind rotors is calculated at various rotor positions and wind speeds through numerical analysis by using SWFS software and TFS. Both methods have been compared with experimental data and presented through figures. The computational study of the performance of the turbine with the same considerations as that of the experimental tests are carried out. For this the computational model as narrated in the last section is considered. As measured experimentally, the static torque was estimated at different wind speed (4, 6 and 8 m/s) and rotor positions (0° to 180°).

To validate the numerical results of SWFS and select a suitable turbulence model to describe the flow parameters around Savonius rotor, comparisons between results of turbulence model, k–ε, and experimental results of Saha et al. [36] has been performed and presented in Table 3. The results show a similar trend in both. The validation study simulation results and the experimental results of Saha et al. [36]. However, Table 3 shows that the numerical results for the mid range of velocities i.e. 6 m/s, 8 m/s, are much more agreeable with the experimental counterparts, where the experimental torque values of Saha et al. [36] are calculated. The reason for difference between the experimental results of Saha et al. [36] and validation study conducted in this paper can be explained from the comparative results of [37] for different turbulence models showing a considerable difference between experimental and numerical results when using SST model for modeling turbulence.

Table 3. Comparison of SWFS results with experimental results of [36]

Inlet velocity [m/s]	Torque [N.m]		Relative error
	Saha et al. [36]	Current work	
6	0.0091	0.016	0.0141
8	0.036	0.043	0.0070

4.2.1. SolidWork Flow Simulation

Figures 11, 12and 13 illustrate the changes of the static torque values related to rotor angle obtained from the model 1, 2 and 3, respectively, through numerical analysis (SWFS) and experiments (EXP) carried out at various wind speeds. It is seen here that the torque values obtained from model 1 through experiment and numerical analysis are higher than model 2 and model 3. The values obtained through numerical analysis have been found to be close to the experimental values, especially for low wind velocity (4 and 6 m/s) compared to highest wind speed (8 m/s). It has been concluded that this case may have been caused by the measurement errors and losses in the experimental study. It is seen from both the experiments and the numerical analysis that static torque of the rotor is rapidly increasing with the increase in wind speed and increase of the bucket arc angle, φ. The results show that predicted values of SWFS model are very close to unity when bucket angle and wind speed decreases as shown in Figures 11, 12 and 13.
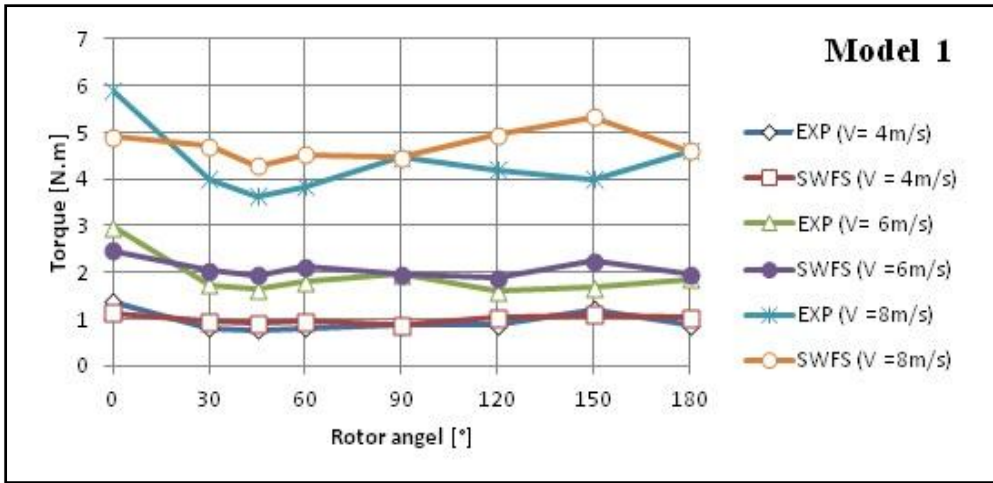
Figure 11. Static torque changes obtained through experiment and SWFS
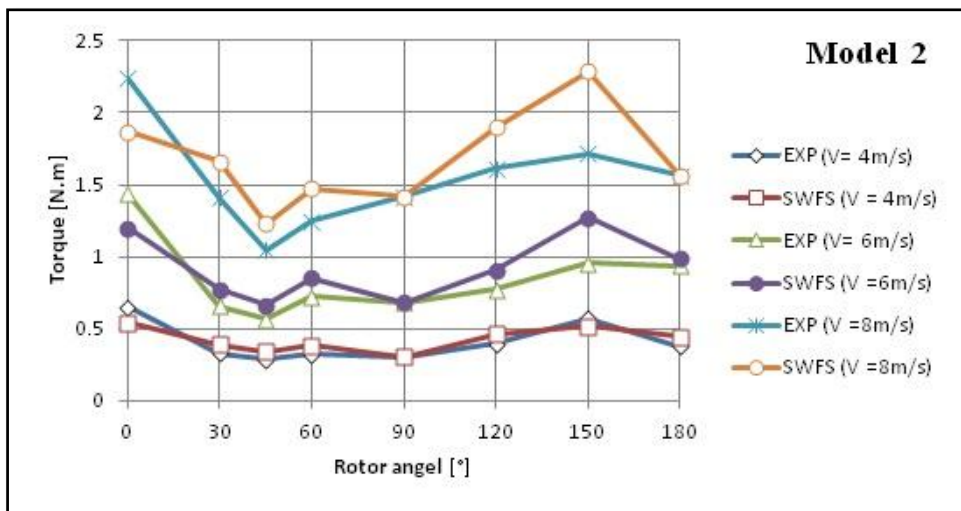for different wind velocity between the value of 0°and 180°

Figure 12. Static torque changes obtained through experiment and SWFS
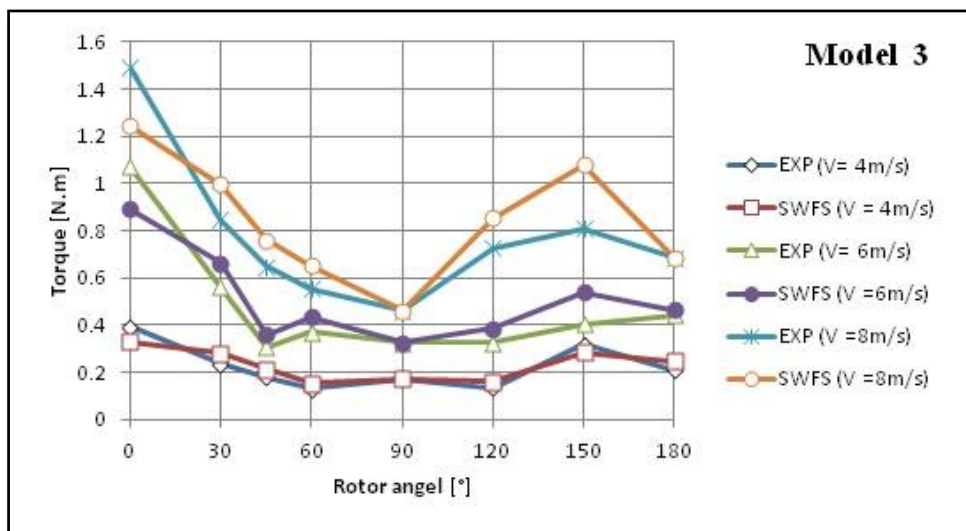for different wind velocity between the value of 0°and 180°

Figure 13. Static torque changes obtained through experiment and SWFS
for different wind velocity between the value of 0°and 180°

4.2.2. Trigonometric Fourier Series (TFS)

The TFS models were developed using MATLAB R2013a with a curve fitting toolbox. Matlab toolbox used experimental static torque data as a function of rotor angle as an input to predict the static torque of models. As an output it gives the static torque of the models at various wind speeds. The list of Trigonometric Fourier Series coefficients and the fundamental frequency of signals with various wind speeds for predicting the static torque of unconventional Savonius wind rotors are shown in Table 4.

Table 4. Lists of Trigonometric Fourier Series coefficients with fundamental frequency
of signal of unconventional Savonius wind models

Models	V = 4 m/s								
	a_0	a_1	b_1	a_2	b_2	a_3	b_3	w	R^2
Model 1	0.929	0.182	0.026	0.178	-0.015	0	0	0.082	0.9691
Model 2	0.397	0.151	-0.049	0	0	0	0	0.0411	0.95
Model 3	0.209	0.0562	0.0318	0.0912	-0.010	0	0	0.0841	0.937
	V = 6 m/s								
	a_0	a_1	b_1	a_2	b_2	a_3	b_3	w	R^2
Model 1	2.213	0.671	-0.458	0.140	-0.511	-0.062	-0.363	0.0202	0.9869
Model 2	0.803	-0.138	-1.817	0.226	-1.919	0.546	-1.818	0.0529	0.9219
Model 3	21.47	-21.08	-18.86	0.6826	7.141	0	0	0.00583	0.9817
	V = 8 m/s								
	a_0	a_1	b_1	a_2	b_2	a_3	b_3	w	R^2
Model 1	6.027	0.938	-2.855	-1.072	-0.933	0	0	0.01926	0.9846
Model 2	1.586	0.199	0.171	0.201	-0.106	0.253	-0.144	-0.0313	0.8831
Model 3	0.779	1.008	-0.343	-0.298	-0.749	0	0	0.0124	0.9677

Figure 13(a), 14(a) and 15(a) show the comparison of the variation of computational torque and experimental torque for model 1, 2 and 3, respectively with respect to rotor angle. Additionally, Figure 13 (b), 14(b) and 15(b) show the results of fittings the predicted and experimental values for torque, respectively using linear regression equations. This (numerical) study clearly shows that the fit values and variance of the results predicted by TFS models has been expressed in terms of *R-square* (R^2) values, which are quite encouraging. R-squared value is a measure of goodness-of-fit, which means how close the data points are to the fitted regression line as shown in Table 4. These values are close to unity, as shown in Figure 13 (b), 14(b) and 15(b), highlighting proper fitting of the predicted values by the adopted methodology
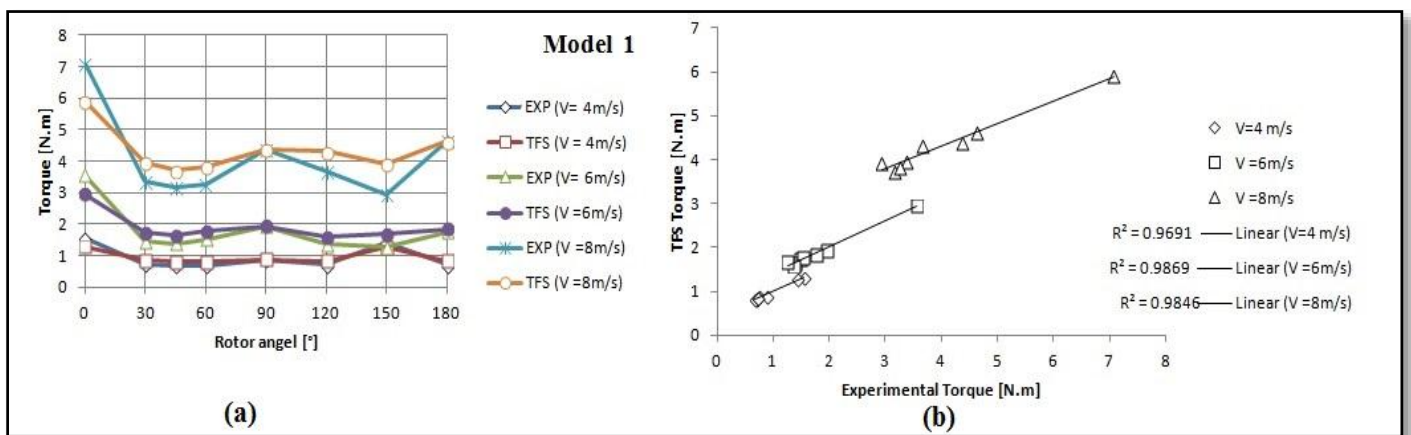

Figure 13. Experimental and computational static torque vs. rotor angle and fitting of the experimental
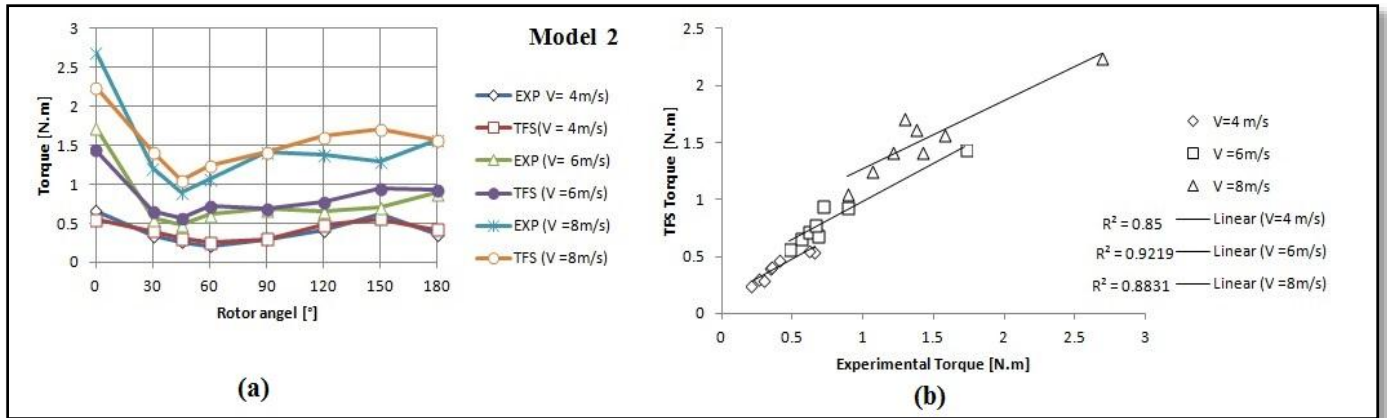and predicted values for model 1

Figure 14. Experimental and computational static torque vs. rotor angle and fitting of the experimental and predicted values for model 2
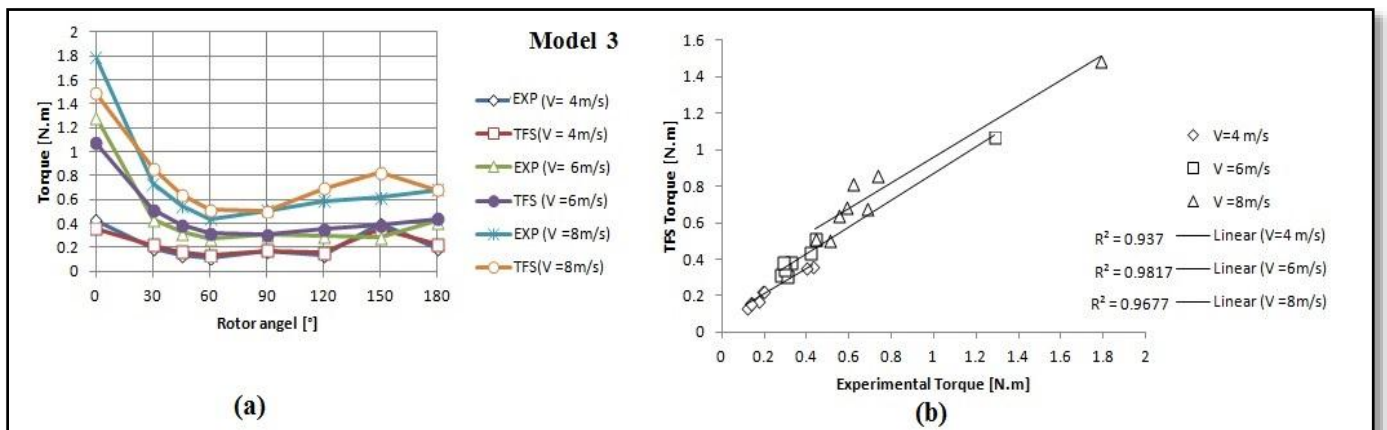

Figure 15. Experimental and computational static torque vs. rotor angle and fitting of the experimental and predicted values for model 3

As a result of the experiments and numerical analysis performed with the rotor using different wind speeds and bucket arc angles, following results are found; The model 1 (bucket arc angle at 90°) has the highest static torque values compared to model 2 and 3. Consequently, Model 1 can provide a better performance than the other rotors. In addition, wind turbine model with bucket arc angle at 90° has more drag force at any position when the wind rotor is in rotational position. Wind turbine rotor with high bucket arc angle will deliver higher torque for the shaft of the rotor. Therefore, model 1, has significant static torque at lower wind speed and more stable at a wind speed of 4 and 6 m/s. It is also observed from the experimental and numerical results, the static torque of the rotors is proportional to the bucket arc angle and wind speed. From the obtained outcomes, it can be concluded that when the arc bucket angle is increased, the performance and efficiency of the rotor are significantly improved. It was observed that for different configurations investigated, model 1 (φ =90°) can increase the average static torque of the unconventional Savonius rotors of 0.227 N.m to 1N. m at 4m/s, 0.5 N.m to 1.9 N.m at 6 m/s and 0.78 N.m to 4.34 N.m at 8m/s. Hence, the power of the rotor can be increased to about 75% with the optimum arc bucket angle. In addition,

this is fairly good value and higher than that obtained with other studies in the literature which was applied for different modifications on the Savonius rotors.

5. CONCLUSIONS AND FUTURE WORKS

In this paper, the static torque of unconventional Savonius wind rotors for three different models was investigated experimentally and numerically. For numerical analysis, the SolidWork Flow Simulation software program and Trigonometric Fourier Series were used. This study compares different design of rotors characterized by the bucket arc angles of φ= 60°, φ=75°and φ= 90° at different wind speed levels, when the others geometrical parameters are fixed. The main outcomes of these actions are outlined below

- It is observed that the unconventional Savonius rotor is sensitive to arc bucket angles and wind speed.

- According to the obtained results, it has been observed that the bucket design has a direct effect on the static torque characteristics.

- The comparison between the results obtained through experiments and numerical analysis has shown that the torque of the rotor increases with increasing the wind speed and it gets greater as the bucket arc angle (φ) increases.

- The new configuration of Savonius rotors that shows the best performance is the one where bucket arc angle 90° and wind speed 8 m/s.

- According to the results, model 1 could be increasing the static torque about 75% with the given conditions which leads to increase the power of the rotor.

- The study showed the best model to use is model 1. It is more efficient and suitable for use by small domestic housing and commercial businesses.

- The R-squared (R^2) values in the linear regression examination of static torque predictions with respect to their experimental values are close to unity, thus highlighting proper fitting of the predicted values by TFS.

- As the experimental and numerical results are greatly closer to each other, the choices of model, and methods used in numerical models are suitable for this study.

In this study, the effects of bucket design performance of unconventional Savonius wind rotors are investigated through experimental and numerical analysis. Thus, as future work, the effects of the blade material and blade geometries on mechanical power of the wind turbine rotor may be well studied.

ACKNOWLEDGEMENTS

REFERENCES

[1]. Mathew, S. (2006). Wind energy: Fundamentals, resource analysis, and economics. Berlin: Springer.

[2]. Hemami , A. (2012). Wind Turbine Technology, Unite State of America. Cengage Learning.

[3]. Savonius SJ. The S-rotor and its application. MechEng 1931; 53:333-8.

[4]. Twidwell JW, Weir AD. Renewable energy resources. The University Press Cambridge, Britain; 1985. 1-411.

[5]. Eldridge FR. Wind machines. Newyork: Van Nostrand; 1980. 1-214.

[6]. Kacprzak, K., Liskiewicz, G., &Sobczak, K. (2013). Numerical investigation of conventional and modified Savonius wind turbines. *Renewable Energy*, *60*, 578-585. doi:10.1016/j.renene.2013.06.009

[7]. Roy, S., &Saha, U. K. (2015). Wind tunnel experiments of a newly developed two-bladed Savonius-style wind turbine. *Applied Energy*, *137*, 117-125. doi:10.1016/j.apenergy.2014.10.022

[8]. Sharma, S., & Sharma, R. K. (2016). Performance improvement of Savonius rotor using multiple quarter blades – A CFD investigation. *Energy Conversion and Management*,*127*, 43-54. doi:10.1016/j.enconman.2016.08.087

[9]. Mohamed, M., Janiga, G., Pap, E., &Thévenin, D. (2011). Optimal blade shape of a modified Savonius turbine using an obstacle shielding the returning blade. *Energy Conversion and Management*, *52*(1), 236-242. doi:10.1016/j.enconman.2010.06.070

[10]. Mahmoud, N., El-Haroun, A., Wahba, E., &Nasef, M. (2012). An experimental study on improvement of Savonius rotor performance. *Alexandria Engineering Journal*, *51*(1), 19-25. doi:10.1016/j.aej.2012.07.003

[11]. Tartuferi, M., D'Alessandro, V., Montelpare, S., & Ricci, R. (2015). Enhancement of Savonius wind rotor aerodynamic performance: a computational study of new blade shapes and curtain systems. *Energy*, *79*, 371-384. doi:10.1016/j.energy.2014.11.023

[12]. Lee, J., Lee, Y., & Lim, H. (2016). Effect of twist angle on the performance of Savonius wind turbine. *Renewable Energy*, *89*, 231-244. doi:10.1016/j.renene.2015.12.012

[13]. Nasef, M., El-Askary, W., AbdEL-hamid, A., & Gad, H. (2013). Evaluation of Savonius rotor performance: Static and dynamic studies. *Journal of Wind Engineering and Industrial Aerodynamics*, *123*, 1-11. doi:10.1016/j.jweia.2013.09.009

[14]. Saha, U., Thotla, S., &Maity, D. (2008). Optimum design configuration of Savonius rotor through wind tunnel experiments. *Journal of Wind Engineering and Industrial Aerodynamics*, *96*(8-9), 1359-1375. doi:10.1016/j.jweia.2008.03.005

[15]. Roy, S., &Saha, U. K. (2015). Wind tunnel experiments of a newly developed two-bladed Savonius-style wind turbine. *Applied Energy*, *137*, 117-125. doi:10.1016/j.apenergy.2014.10.022

[16]. Kang, C., Liu, H., & Yang, X. (2014). Review of fluid dynamics aspects of Savonius-rotor-based vertical-axis wind rotors. *Renewable and Sustainable Energy Reviews*, *33*, 499-508. doi:10.1016/j.rser.2014.02.011

[17]. Akwa, J. V., Alves da Silva Júnior, G., &Petry, A. P. (2012). Discussion on the verification of the overlap ratio influence on performance coefficients of a Savonius wind rotor using computational fluid dynamics. *Renewable Energy*, *38*(1), 141-149. doi:10.1016/j.renene.2011.07.013

[18]. Driss, Z., Damak, A., &Abid, M. S. (2015). Evaluation of the Savonius Wind Rotor Performance for Different External Overlap Ratios. *International Journal of Fluid Mechanics & Thermal Sciences*, *1*(1), 14. doi:10.11648/j.ijfmts.20150101.13

[19]. Mohamed, M., Janiga, G., Pap, E., &Thévenin, D. (2010). Optimization of Savonius turbines using an obstacle shielding the returning blade. *Renewable Energy*, *35*(11), 2618-2626. doi:10.1016/j.renene.2010.04.007

[20]. Wenehenubun, F., Saputra, A., &Sutanto, H. (2015). An Experimental Study on the Performance of Savonius Wind Turbines Related With The Number Of Blades. Energy Procedia, 68, 297-304. doi:10.1016/j.egypro.2015.03.259

[21]. Roy, S., &Saha, U. K. (2013). Review on the numerical investigations into the design and development of Savonius wind rotors. *Renewable and Sustainable Energy Reviews*, *24*, 73-83. doi:10.1016/j.rser.2013.03.060

[22]. Kianifar, A., Anbarsooz, M., &Javadi, M. (2010). Blade Curve Influences on Performance of Savonius Rotors: Experimental and Numerical. *ASME 2010 3rd Joint US-European Fluids Engineering Summer Meeting: Volume 1, Symposia – Parts A, B, and C.* doi:10.1115/fedsm-icnmm2010-30919

[23]. Kianifar, A., &Anbarsooz, M. (2011). Blade curve influences on the performance of Savonius rotors: experimental and numerical. *Proceedings of the Institution of Mechanical Engineers, Part A: Journal of Power and Energy*, *225*(3), 343-350. doi:10.1177/2041296710394413

[24]. Lin, C., &Klimina, L. A. (2014). CFD simulation and analysis for Savonius rotors with different blade configuration. doi:10.1063/1.4904626

[25]. Muscolo, G. G., &Molfino, R. (2014). From Savonius to Bronzinus: A Comparison among Vertical Wind Turbines. *Energy Procedia*, *50*, 10-18. doi:10.1016/j.egypro.2014.06.002

[26]. Driss, Z., Mlayeh, O., Driss, S., Driss, D., Maaloul, M., & Abid, M. S. (2015). Study of the bucket design effect on the turbulent flow around unconventional Savonius wind rotors. *Energy*, *89*, 708-729. doi:10.1016/j.energy.2015.06.023

[27]. Driss, Z., Mlayeh, O., Driss, D., Maaloul, M., &Abid, M. S. (2014). Numerical simulation and experimental validation of the turbulent flow around a small incurved Savonius wind rotor. *Energy*, *74*, 506-517. doi:10.1016/j.energy.2014.07.016

[28]. Frikha, S., Driss, Z., Ayadi, E., Masmoudi, Z., &Abid, M. S. (2016). Numerical and experimental characterization of multi-stage Savonius rotors. *Energy*, *114*, 382-404. doi:10.1016/j.energy.2016.08.017

[29]. Kamoji, M., Kedare, S., &Prabhu, S. (2009). Performance tests on helical Savonius rotors. Renewable Energy, 34(3), 521-529. doi:10.1016/j.renene.2008.06.002

[30]. Driss, Z., Bouzgarrou, G., Chtourou, W., Kchaou, H., &Abid, M. (2010). Computational studies of the pitched blade turbines design effect on the stirred tank flow characteristics. *European Journal of Mechanics - B/Fluids*, *29*(3), 236-245. doi:10.1016/j.euromechflu.2010.01.006

[31]. Ammar, M., Chtourou, W., Driss, Z., &Abid, M. (2011). Numerical investigation of turbulent flow generated in baffled stirred vessels equipped with three different turbines in one and two-stage system. *Energy*, *36*(8), 5081-5093. doi:10.1016/j.energy.2011.06.002

[32]. Driss, Z., Karray, S., Kchaou, H., & Abid, M. (2011). CFD simulation of the laminar flow in stirred tanks generated by double helical ribbons and double helical screw ribbons impellers. *Open Engineering*, *1*(4). doi:10.2478/s13531-011-0034-5

[33]. Lam, C. K., &Bremhorst, K. (1981). A Modified Form of the k-ε Model for Predicting Wall Turbulence. *Journal of Fluids Engineering*, *103*(3), 456. doi:10.1115/1.3240815

[34]. Frikha, S., Driss, Z., &Hagui, M. A. (2015). Computational study of the diffuser angle effect in the design of a waste heat recovery system for oil field cabins. *Energy*, *84*, 219-238. doi:10.1016/j.energy.2015.02.090

[35]. Tolstov, G. P., & Silverman, R. A. (1976). Fourier Series. New York: Dover Publications.

[36]. Saha, U., Thotla, S., & Maity, D. (2008). Optimum design configuration of Savonius rotor through wind tunnel experiments. *Journal of Wind Engineering and Industrial Aerodynamics*, *96*(8-9), 1359-1375. doi:10.1016/j.jweia.2008.03.005

[37]. Mohamed, M., Janiga, G., Pap, E., & Thévenin, D. (2011). Optimal blade shape of a modified Savonius turbine using an obstacle shielding the returning blade. *Energy Conversion and Management*, *52*(1), 236-242. doi:10.1016/j.enconman.2010.06.070